Dipole based model of static and dynamic forces in ironless drives with active control of 6DOF

Karlo RADMAN*, Wolfgang GRUBER**, Hubert Mitterhofer*
*Area Drives, Linz Center of Mechatronics GmbH, Austria
**Institute of Electric Drives and Power Electronics, Johannes Kepler University Linz, Austria *Japan Society of Mechanical Engineers

Abstract

This research covers the magnetic dipole-based modelling of ironless levitating systems with 6 actively controlled degrees of freedom. As the system contains only permanent magnets and electrical conductors it can be modelled without the need to solve the differential Maxwell's equations, in the model region with a finite element mesh, but by using a point-cloud based approach. The electromagnetic solver is implemented using only basic vector operations without any linear algebra or iterative processes. The permanent magnet segments are represented by point dipole magnets, and the conductors by point current sources. Any shape of magnets and coils can be modeled or imported from another finite element solver. A simulation model will be shown including the computation of the force, torque, magnetic flux and the eddy current losses in the stator coils. The dynamic performance of the drive is considered, and an improved system is shown based on reduced eddy losses. The analysis considers the weight, acceleration and moving speed of the drive.

Keywords : planar drive, magnetic levitation, dipole model, eddy-currents, iron-less system, dynamic losses

1. Introduction

This paper presents a simulation workflow for ironless planar levitating drives. Due to the linear nature of ironless systems, the superposition of magnetic field contributions is possible, and has been used in multiple solver implementations. A permanent magnet (PM) can be described by a surface charge model, a surface current model (Trumper et al., 1996), a harmonic field distribution around the permanent magnet array (Boeij, 2006) or by a magnetic dipole model [Marth et al., 2014]. This research focuses on the point cloud representation of dipoles for the PMs and point current sources for the conductors. Arbitrary shapes with non-homogeneous magnetizations/currents can be simulated, which is not the case in the previously mentioned solvers working only with simple shapes. For triangular meshed surfaces, the surface current model can be used on source free regions as presented in Mäkinen et al., 2020. Another solution is to reduce shapes into simpler and express each contribution by a harmonic model (Zhang and Kou, 2017). The implemented solver is used for planar levitating drives, as depicted in Fig. 1 and Jansen et.al., 2008. The force acting on the magnetic array (shuttle), the linked fluxes and eddy current (EC) losses are computed with the dipole solver.

2. Dipole Model

The dipole model can represent any arbitrary PM shape with non-homogeneous magnetizations. The PM object is represented by a set of discrete volume subdivisions Ω_m, each defined by its relative position vector $\boldsymbol{r_m}$ and magnetic moment $\boldsymbol{m_m}$. Likewise, the electrical conductors are defined by point current sources Ω_c, each with a defined relative position $\boldsymbol{r_c}$ and point current $\boldsymbol{j_c}$. A single magnet and conductor discrete point is shown in Fig. 2. The dipole moment and point current vector for each element are defined by the remanence $\boldsymbol{B_r}$ and current density $\boldsymbol{J}$, respectively. Both values are scaled by the volume of the subdivisions, V_m in case of PM and V_c in case of conductors:

$$\boldsymbol{m_m} = \frac{1}{\mu_0}\boldsymbol{B_r}V_m \tag{1}$$

$$\boldsymbol{j_c} = \boldsymbol{J}V_c \tag{2}$$

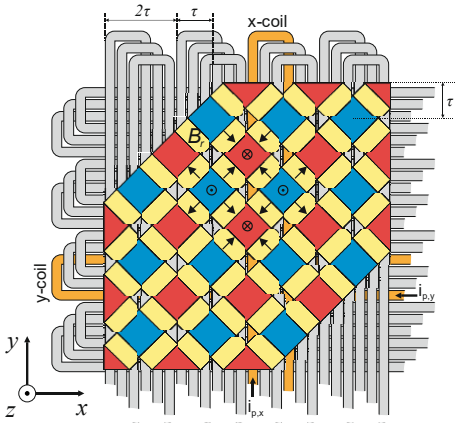

Fig. 1 A planar drive with a stator of interleaving elongated coils along the *x*- and *y*-axis. Above the stator is the levitating PM array with a checkered Halbach arrangement with a pole pitch of τ.

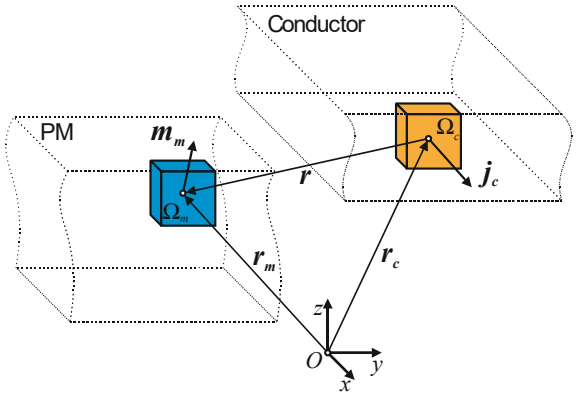

Fig. 2 Sub elements in the solver, a dipole and point current source. The whole system is described by the positional vectors $\boldsymbol{r_m}$ and $\boldsymbol{r_c}$, and the dipole moment $\boldsymbol{m_m}$ and point current $\boldsymbol{j_c}$.

The magnetic moments are in units of ampere per square meter (A/m²) while the point currents are in ampere meters (Am), also used to express magnetic pole strength. For a modeled looped conductor, a coil, the connecting terminals are ignored and the integral of $\boldsymbol{j_c}$ over all Ω_c, must be equal to 0, as to adhere to Ampère's law. With a constant cross section of the conductor, any single or multi-turn coil can be assumed to have a constant current density, with the vector $\boldsymbol{J}$ always pointing normal to the cross section**.** In case of conductors with a varying cross-section, as in e.g. PCB traces with vias, the current density within the conductor can be initially solved in another magnetostatic FEM solver and converted into a point current representation by taking the volume and a $\boldsymbol{J}$ in each mesh element.

Concerning the PM, the curl of the magnetic vector potential $\boldsymbol{A_m}$ is the magnetic flux density $\boldsymbol{B_m}$ around an infinitesimally small current loop or dipole

$$\boldsymbol{B_m}(\boldsymbol{r}) = \boldsymbol{\nabla} \times \boldsymbol{A_m}(\boldsymbol{r}) = \boldsymbol{\nabla} \times \left(\frac{\mu_0}{4\pi}\frac{\boldsymbol{m_m} \times \boldsymbol{r}}{|\boldsymbol{r}|^3}\right) = \frac{\mu_0}{4\pi}\left(\frac{3\boldsymbol{r}\,(\boldsymbol{m_m} \cdot \boldsymbol{r})}{|\boldsymbol{r}|^5} - \frac{\boldsymbol{m_m}}{|\boldsymbol{r}|^3}\right), \tag{3}$$

where the vector $\boldsymbol{r}$ represents the direction from the PM dipole position $\boldsymbol{r_m}$ to an arbitrary evaluation point in space, usually a conductor element Ω_c. In the case of conductors, the magnetic flux density $\boldsymbol{B_c}$ around them can be expressed using the Biot-Savart law with the vector $\boldsymbol{r}$ now pointing outwards from the point current source

$$\boldsymbol{B_c}(\boldsymbol{r}) = \frac{\mu_0}{4\pi}\frac{\boldsymbol{j_c} \times \boldsymbol{r}}{|\boldsymbol{r}|^3}\,. \tag{4}$$

2.1 Force computation

The force can be either defined as exerted on the conductor by magnet ($\boldsymbol{F_{m\to c}}$) which is the Laplace force $\boldsymbol{j_c} \times \boldsymbol{B_m}$ or exerted on a dipole Ω_m by the field generated by the coil element ($\boldsymbol{F_{c\to m}}$). In the latter case the force acting on a PM element, generated by a conductor element is equal to

$$\boldsymbol{F_{c\to m}}(\boldsymbol{r}) = \boldsymbol{\nabla}(\boldsymbol{m_m} \cdot \boldsymbol{B_c}(\boldsymbol{r})) = \frac{\mu_0}{4\pi}\left(\frac{\boldsymbol{j_c} \times \boldsymbol{m_m}}{|\boldsymbol{r}|^3} - 3\frac{(\boldsymbol{j_c} \times \boldsymbol{r})(\boldsymbol{m_m} \cdot \boldsymbol{r})}{|\boldsymbol{r}|^5}\right). \tag{5}$$

The above equation is evaluated for each Ω_m of the PM and each Ω_c of the coil to get the total force. For PM and coil objects dived in n_m and n_c elements respectively, all vectors $\boldsymbol{m_m}$ are packed together in a $n_m \times 3$, and all $\boldsymbol{j_c}$ vectors in a $n_c \times 3$ matrix. All relative position vectors $\boldsymbol{r}$ are therefore included in a $n_m \times n_c \times 3$ matrix. The force equation between a coil and a magnet assembly are solved by vector and matrix operations without the need to iterate over the sub-elements. If the force between two movers is computed, the $\boldsymbol{B_c}$ is replaced by the field of a second magnet array in Eq. (5).

The torque is calculated directly from the force exerted on each Ω_m element. The torque acting on a magnet dipole consists of the torque due to the exerted forces around the arbitrary center of rotation $\boldsymbol{r_f}$, and the torque exerted on the dipole by an external field, like the one generated by a coil in Eq.(4)

$$\boldsymbol{T_{c\to m}}(\boldsymbol{r}) = \boldsymbol{r_f}(\boldsymbol{r}) \times \boldsymbol{F_{c\to m}}(\boldsymbol{r}) + \boldsymbol{m_m} \times \boldsymbol{B_c}(\boldsymbol{r})\,. \tag{6}$$

3. Flux linkage

The flux linkage Ψ, and its derivative, the induced electromotive force $\mathcal{E}$, that a magnet array exerts in a coil can be computed by using the vector potential $\boldsymbol{A_m}$ from Eq. (3) and the Kelvin–Stokes theorem (Trumper et al., 1996)

$$\Psi = \oiint \boldsymbol{\nabla} \times \boldsymbol{A_m}(r) \cdot \mathrm{d}S = \oint \boldsymbol{A_m}(\boldsymbol{r}) \cdot \mathrm{d}\boldsymbol{l} = \oint \boldsymbol{A_m}(r) \cdot \hat{\boldsymbol{J}}\, \mathrm{d}l \ . \tag{7}$$

From the right expression in Eq. (7) the unit vector of the current density $\boldsymbol{J}$ can be expressed from Eq. (2) as the division of the unit vector of the element current $\boldsymbol{j_c}$ by the element volume V_c. Figure 3. shows the coil definition with cuboid elements Ω_c. As the shape of the subdivision elements is not strictly defined the discrete dl length is undefined. The integral solution can then be found by dividing the element volume V_c by the cross-section surface of the conductor A_{cond}. This way the elements, which are parallel in the current path, are scaled in their contribution along the integration path. Converting the integration to the summation of the n_c coil elements, and summing the contribution of all n_m PM parts leads to the implemented flux linkage equation based on vector operations

$$\Psi = \sum_{c=1}^{n_c} \left(\sum_{m=1}^{n_m} \mathbf{A_m}(\mathbf{r}) \cdot \frac{\hat{\mathbf{j}}_\mathbf{c}}{V_c} \right) \frac{V_c}{A_{cond}} = \frac{\mu_0}{4\pi A_{cond}} \sum_{c=1}^{N_c} \sum_{m=1}^{N_m} \frac{(\mathbf{m_m} \times \mathbf{r}) \cdot \hat{\mathbf{j}}_\mathbf{c}}{|\mathbf{r}|^3} \ . \tag{8}$$

The induced electromotive force can be computed from the flux derivative over time or over the position at a constant speed. In the case of the magnetic array moving at a constant speed v_x along the x-axis we have

$$\mathcal{E} = \frac{\mathrm{d}\Psi}{\mathrm{d}t} = \frac{\mathrm{d}\Psi}{\mathrm{d}\boldsymbol{x}} \boldsymbol{v_x} \ . \tag{9}$$

In Fig. 2, only the vertical coils marked x-coils will have a considerable induced voltage in them, and the perpendicular y-coils will only experience an induced voltage if the magnet array has a speed component along the y-axis. The coupling inductance between the stator coils can be computed in the same way as the linked flux in Eq. (7) by replacing $\boldsymbol{A_m}$ with the vector potential generated by neighboring coils.

3.1 Eddy current approximation by conductor flux linkage

If relatively wide conductors are used, as in the case with printed circuit board (PCB) layers, the eddy currents induced in the copper are not negligible. In a standard three phase coil arrangement, shown in Fig. 2, the coils are as wide as a third of the pole pitch τ. If the coils are created with a single turn per layer, the conductor is also a third of τ. The eddy currents loops are formed in the conductors in the xy-plane. A simplified loop form used in the estimation is shown in Fig. 4. The eddy current losses in a transient FEM solver are computed by the current density in the mesh of the conductive material. The losses can be expressed by a eddy current loop current $\boldsymbol{i_{ec}}$ and loop resistance R_{ec}

$$P_{ec} = \rho \int J^2 \mathrm{d}V = R_{ec} i_{ec}^2 \ . \tag{10}$$

To keep the solver implementation fast and vector based, an solution is presented for the estimation of the eddy-currents. Equation (7) can be rewritten as for a loop with a voltage source u_{ec}. The voltage can be approximated as a linked flux on A_{ec}, half of the conductor surface A_{cond}, and along a path that circles back inside the conductor.

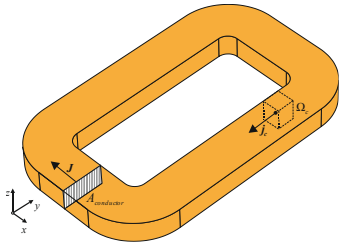

Fig. 3 Definition of a basic coil in the dipole solver. The cross section A_{cond} is kept constant, as to also keep the current density $\boldsymbol{J}$ constant, and simplify the definition of the point currents $\boldsymbol{j_c}$

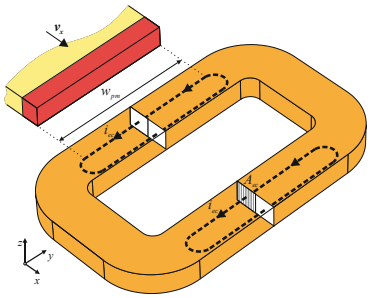

Fig. 4 The simplified solver model of eddy currents. Each conductor is treated as a coil in which the loop closes. The size of the loop is determined by the width of the magnet array w_{pm} moving above the conductors.

The eddy current flux linkage is computed only for the straight part of the loop, each occupying a half of the conductor. Combining Eq (10) with Eq. (8) we can express the approximated losses at a constant v_x speed as

$$\boldsymbol{P}_{\boldsymbol{ec,dipole}} \approx \frac{u_{ec}^2}{R_{ec}} = \frac{1}{R_{ec}}\left(\frac{\mathrm{d}\Psi_{ec}}{\mathrm{d}\boldsymbol{x}}\right)^2 \boldsymbol{v_x} = \frac{\mu_0 \boldsymbol{v_x}}{4\pi A_{ec} R_{ec}}\left(\frac{\mathrm{d}}{\mathrm{d}\boldsymbol{x}}\left(\sum_{ec=1}^{\mathrm{Nec}}\sum_{m=1}^{N_m}\frac{(\boldsymbol{m_m}\times\boldsymbol{r})\cdot\widehat{\boldsymbol{i_{ec}}}}{|\boldsymbol{r}|^3}\right)\right)^2 . \tag{11}$$

The only variable not yet defined in Eq. (11) is the resistance of the loop R_{ec}. This resistance is approximated with the resistance of the straight part of the loop with the length equal to the magnet width w_{pm} and two correctional factors $k_{end,ec}$ and $k_{l,ec}$. Figure 5. shows the simulated induced eddy current in the transient FEM solver with parameters listed in Table 1.

As the loop-end shape is not known, their influence on the resistance is assessed by Eq. (12) from different w_{pm} cases solved with the transient Ansys Maxwell 3D solver (Table 2). After the loop end contribution $k_{end,ec}$ has been found to be an increase to the resistance, the effective length $k_{l,ec}$ has been computed to be ~79%, as seen in the comparison in Table 3. The computed factors are only valid for similar thin and wide conductors. For other shapes they need to be recomputed as in the case of the loop end contribution

$$k_{end,ec}(w_{pm}) = 1 - \frac{P_{ec,3Dfem}(w_{pm})}{P_{ec,3Dfem}(2w_{pm}) - P_{ec,3Dfem}(w_{pm})} \approx \frac{2.3\,\tau}{w_{pm}}. \tag{12}$$

With these loop correction factors we can approximate the resistance of the loop as

$$R_{ec} = \rho\frac{2w_{pm}\,k_{l,ec}}{A_{ec}\,(1-k_{end,ec})} = \rho\frac{2w_{pm}\,k_{l,ec}}{A_{ec}\,(1-\frac{2.3\,\tau}{w_{pm}})}. \tag{13}$$

Table 1. Parameters of the conductor traces and magnet array used for the eddy current assessment

Magnet pole pitch τ	18mm
Number of poles n_m	3
Magnet height h_m	6mm
Conductor width w_c	5.5mm
Conductor height h_c	0.3mm
Conductor length l_c	180mm
Traces in stack n_{turns}	6
Layer isolation h_{iso}	0.2mm
Airgap δ	1mm
Speed along the x-axis v_x	1m/s

Table 2. 3D FEM eddy current losses vs. magnet length.

w_{pm} [τ]	$P_{ec,3Dfem}$ [mW]	ΔP_{ec} from linear [mW]	Loop end factor $k_{end,ec}$ [%]
1.5	125	-23	15.33
3	272	-23	7.67
6	568	-23	3.83

Table 3. Scaling between the 3D FEM and approximated dipole model losses

w_{pm} [τ]	$P_{ec,3dfem}$	$P_{ec,dipole}$ linear	$P_{ec,dipole}$ incl. $k_{end,ec}$ [mW]	Effective length factor $k_{l,ec}$ [%]
6	568mW	466mW	448mW	79

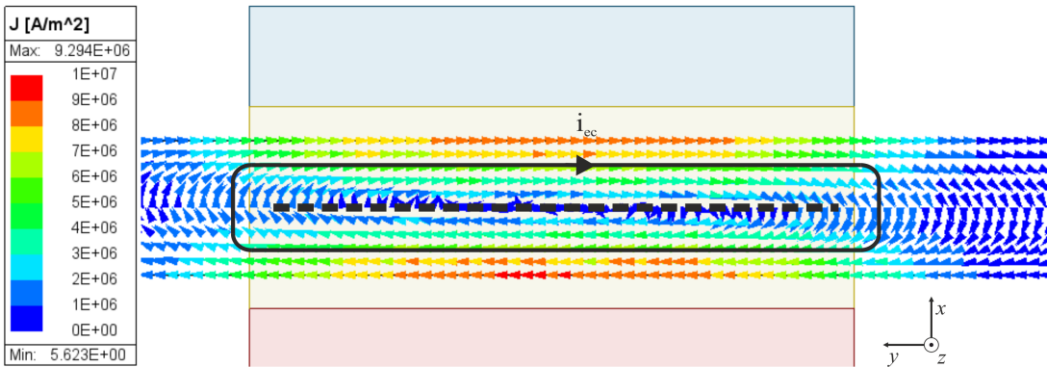

Fig. 5 Eddy currents vectors in a conductor with a shuttle moving over it along the *x*-axis, in a Ansys 3D transient simulation. The added simplified current loop over it is the approximation used in the dipole solver. The loop length factor is approximated from one full 3D simulation at a constant speed and airgap height

The following Fig. 6 and Fig. 7 show that the dipole solver computes the eddy-current loop flux and the voltage with very good overlap to the 2D and 3D transient FEM solvers. Compared to the 3D FEM Ansys solver, the dipole computation is about two orders of magnitude faster. Figure 4. show the resulting approximated eddy losses using Eq. (11). The average losses are the same with a slight over- and undershoot in the simplified dipole model. On a stator densely populated with coils, as in Fig. 1, the per conductor losses add up to a constant term, which leads to a constant braking force, e.g. along the x-axis

$$\bar{F}_{ec,x} = \frac{\bar{P}_{ec,x}}{v_x} \,. \tag{14}$$

This force needs to be counteracted during the shuttle movement, leading to excess phase ohmic losses as well as the eddy current losses in the coils. One option to reduce the losses is to reduce the size of the eddy current loops. By changing the coil shape to two turns per layer, the surface A_{ec} is halved. Simulations show that it leads to 8 times smaller losses per conductor, but as the number of conductors has doubled, there is an effective 4 time reduction in the eddy losses. Figure 9. Shows such an arrangement in a PCB coil.

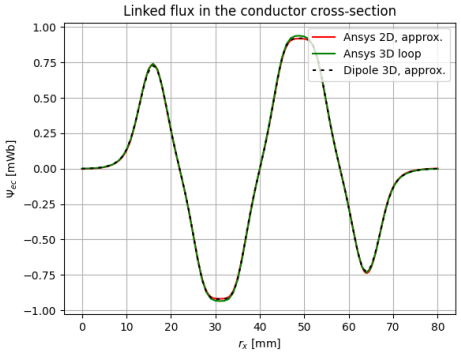

Fig. 6 Linked flux in a approximated eddy current loop. The Ansys 2D implementation uses the same assumption as the dipole solver and the results are identical. The Ansys 3D loop is a conductor split in the middle acting as a coil from Fig. 4

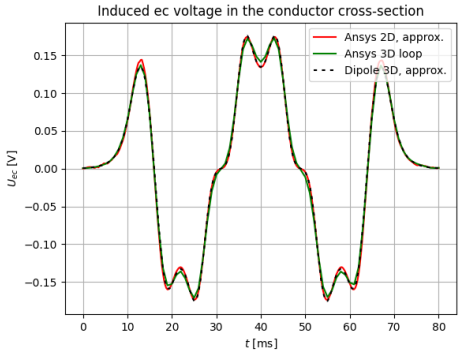

Fig. 7 Derivative of the linked flux in the eddy current loop approximation. All results are identical without any scaling as they represent the same loop.

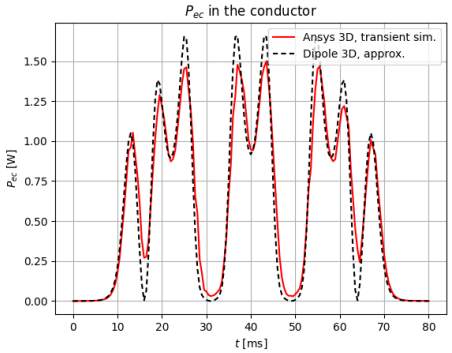

Fig. 8 The eddy-current losses of a single conductor. The simplified eddy-loop approximation is a good match for the detailed 3D FEM simulation of the losses.

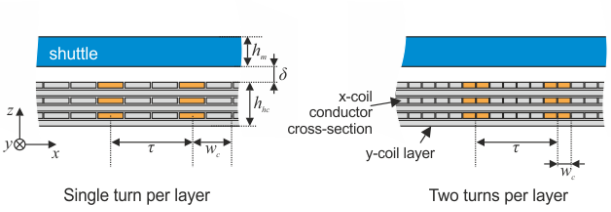

Fig. 9 Coil layer stack with a single or two turns per layer. With double turns per layer the eddy losses are 4 times smaller. Due to the isolation between conductors in a layer, the resistance does not proportionally increase.

5. Planar drive controllability

Each elongated coil on the stator can generate a normal and tangential force. For the x-coils (Fig. 1), those are the forces in x- and z-axis direction, and for group y-coils the forces in y- and z-axis direction. The rotational DOFs around the x- and y-axis can be exerted by opposing F_z generated on the edges of the shuttle. To exert a rotational torque around

the z-axis, the F_x and F_y vectors generated on opposing sides of the shuttle need to be centrally symmetric but not parallel to the torque arm, leading to the slanted/diagonal shuttle shape in Fig. 1.

If we define the force vector for the translator as

$$Q = \left[F_x\ F_y\ F_z\ T_x\ T_y\ T_z\right]^T, \tag{15}$$

and the currents of the underlying stator as

$$i_s = [i_1\ i_2\ \cdots i_n]^T, \tag{16}$$

we can express the active force generation by the linear expression

$$Q = T_m(r)i_s\ , \tag{17}$$

where $\boldsymbol{r}$ is the relative position and orientation of the shuttle

$$r = [x_m\ \ y_m\ \ z_m\ \ \alpha_m\ \ \beta_m\ \ \gamma_m]. \tag{18}$$

The T_m is the matrix of force and torque contributions per each coil and per 1 A current, at each position $\boldsymbol{r}$ of the translator in the operating volume. All 6 DOF force and torque characteristics in the operational symmetric area are assessed to create the T_m matrix. To evaluate a generalized magnetic bearing system with an arbitrary number of phases, the pseudo-inverse control matrix is used. The inverse of T_m links the phase currents from the controller to the output forces Q that need to be exerted on the shuttle,

$$i_s = {T_m}^{-1}Q = K_mQ\ . \tag{19}$$

The conventional solution is reached by using the Moore–Penrose inverse, which minimizes the least squares and therefore minimizes the ohmic losses of the system (Lierop et al., 2006)

$$K_m = {T_m}^T(T_m{T_m}^T)^{-1}\ . \tag{20}$$

5.1 Loss factors

A set of loss factors are calculated from the computed control matrix. These factors are derived from the K_m entries averaged along the symmetric movement on the stator, at a fixed airgap. For each DOF we have a scalar

$$C_a = \left[C_{a,Fx}\ C_{a,Fy}\ \ C_{a,Fz}\ C_{a,Tx}\ C_{a,Ty}\ C_{a,Tz}\right], \tag{21}$$

proportional to the losses generated by only that DOF exerted. In the case of the force generation along the x-axis, the average F_x losses are proportional to the square of the K_m components

$$C_{a,Fx} = \frac{1}{2\tau}\sum_{j=1}^{n}\int_{-\tau}^{\tau}{K_{j,Fx}}^2\,dx. \tag{22}$$

The average ohmic losses, while only generating a Fx force, can be evaluated from

$$\bar{P}_{Fx} = {i_{s,rms}}^T i_{s,rms}\,R_{coil} = C_{a,Fx}\,{F_x}^2R_{coil}, \tag{23}$$

where R_{coil} is the phase resistance and $i_{s,rms}$ is the vector of effective phase currents needed to generate the F_x force.

6. Dynamic losses

For a shuttle flying at constant speed v_x and applying a force to accelerate by a_x, the ohmic/thermal losses in the coils can be expressed as the eddy current losses and the ohmic losses due to the phase currents

$$\bar{P}_{ohmic} = \bar{P}_{ec,x} + \left(C_{a,Fx}\,{F_x}^2 + C_{a,Fz}\,{F_z}^2\right)R_{coil}\ . \tag{24}$$

The two current/force squares can be added, as the F_x and F_z generating currents are orthogonal. The F_z force is a function of the shuttle mass m_{sh}, while the F_x is a sum of the force to counteract the F_{ec} force Eq. (14) and the acceleration force $m_{sh}{\cdot}a_x$. The eddy losses are scaled by the square of the speed, thus defined by nominal losses at v_{norm} e.g. 1m/s as

$$\bar{P}_{ec,x}(v_x) = \bar{P}_{ec,x,norm}\frac{v_x^2}{v_{norm}^2}\ . \tag{25}$$

Applying all these relations to Eq. (24) we get a function depending on the speed, acceleration and shuttle mass

$$\bar{P}_{ohmic}(v_x, m_{sh}, a_x) = \bar{P}_{ec,x,norm}\frac{v_x^2}{v_{norm}^2} + \left(C_{a,Fx}\left(m_{sh}a_x + \bar{P}_{ec,x,norm}\frac{v_x}{v_{norm}^2}\right)^2 + C_{a,Fz}\,(m_{sh}g)^2\right)R_{coil} \quad . \tag{26}$$

6.1 Reduction of dynamic losses

An option to reduce the losses of a moving shuttle was already hinted at in Fig. 9. By doubling the turns per layer, the eddy losses are reduced by a factor of 4. The K_m factors are halved, reducing the loss factors Eq. (22) to a quarter of the initial case. But the resistance of the double-turn coil also quadrupled leaving Eq. (23) with almost equal ohmic losses in both cases, only increased by the loss of conductor surface

$$R_{coil,double} = 4R_{coil}\frac{A_{cond}}{2A_{cond,double}} = 4R_{coil}\frac{w_c}{2w_{c,double}}. \tag{27}$$

If the starting width of the coil w_c was 5.5mm, the double turns solution will have a w_c of 2mm due to additional trace isolation of 1mm. The phase ohmic losses will increase by 5.5/4 equaling 137.5%. In a static scenario where the shuttle is floating in position, the solution with the double turns is always worse by 37.5%, as seen along the zero speed in Fig. 10 and Fig. 11. But in a dynamic scenario, the reduced eddy current losses show an advantage as presented in Fig. 12 for any load point above ~0.5m/s.

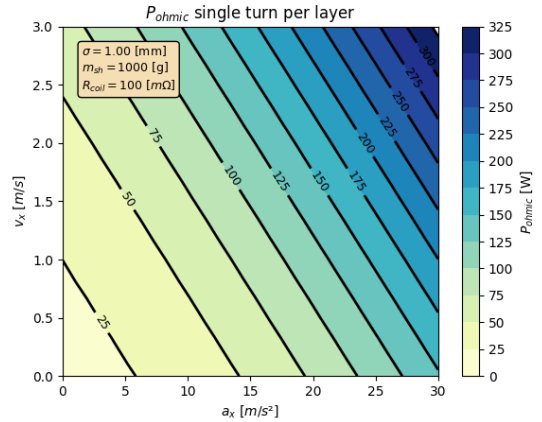

Fig. 10 Ohmic losses in the coils with a single turn per layer. The losses increase by the shuttle speed and applied momentary acceleration

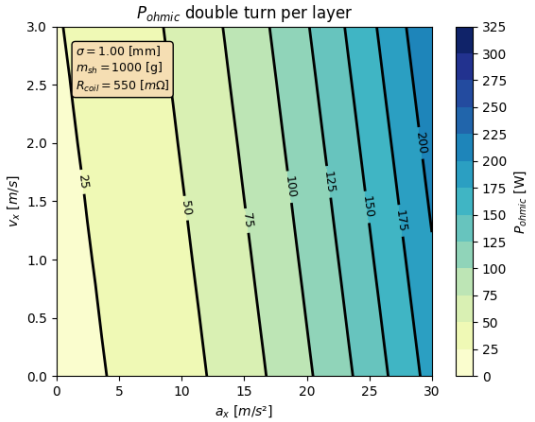

Fig. 11 Ohmic losses in the coils with two turns per layer. The losses increase by the applied momentary acceleration, and are less dependent on the speed

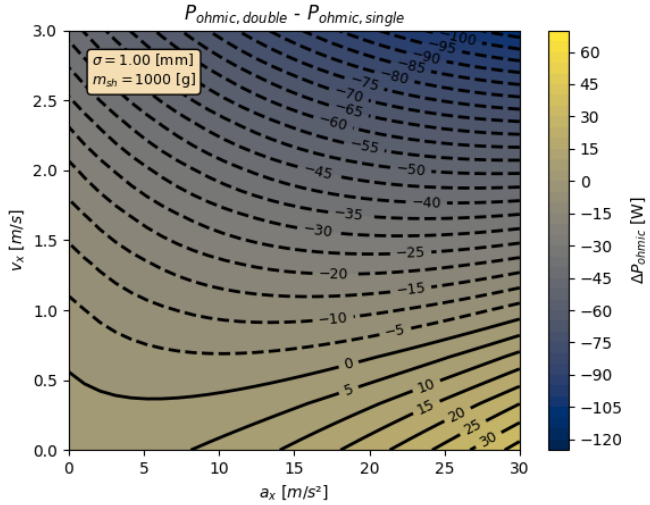

Fig. 8 Difference between the stator with single and double turn per layer. Below ~0.5m/s the single turn coils are better as the coil cross-section is greater. As soon as the shuttle moves above ~0.5m/s, the coils with two turns per layer produce less heat in the coils at the same load

7. Summary

This paper details a novel solver for linear non-ferromagnetic levitating system. It was presented on a planar drive use case, but can also be used on rotational machines, e.g bearingless motors with air coils. Calculation of the forces and losses have been implemented with only vector operations. A set of general control parameters are used to estimate the average losses per DOF and have been applied to evaluate drives with variable mass, speed and acceleration. A coil shape with two turns per layer was proposed and shown to be advantageous if the drive operates above a certain speed.

The force and linked flux computations are around 2 orders of magnitude faster than the same problems in a 3D FEM solver. The proposed estimation of the eddy current losses was shown to be a good match and is used for a whole array of coils. Such an array of layered coils would be hard to simulate with a detailed FE mesh but is no issue in the dipole point cloud solver.

8. Acknowledgement

This work was carried out at LCM GmbH as part of a K2 project. K2 projects are financed using funding from the Austrian COMET-K2 program. The COMET-K2 projects at LCM are supported by the Austrian federal government, the federal state of Upper Austria, Johannes Kepler University Linz, and all partners that form part of the COMET-K2 consortium.

References

Boeij J. de, Lomonova E. and Vandenput A., "Modeling Ironless Permanent-Magnet Planar Actuator Structures," in *IEEE Transactions on Magnetics*, vol. 42, no. 8, (2006), pp. 2009-2016

Jansen J. W., Lierop C. M. M. van, Lomonova E. A. and Vandenput A. J. A., "Magnetically Levitated Planar Actuator with Moving Magnets," in *IEEE Transactions on Industry Applications*, vol. 44, no. 4, (2008), pp. 1108-1115

Lierop C. M. M. van, Jansen J. W., Damen A. A. H. and Bosch P. P. J. van den Bosch, "Control of multi-degree-of-freedom planar actuators," 2006 IEEE Conference on Computer Aided Control System Design, 2006 IEEE International Conference on Control Applications, 2006 IEEE International Symposium on Intelligent Control, Munich, Germany, (2006), pp. 2516-2521

Marth E., Jungmayr G. and Amrhein W., "A 2-D-Based Analytical Method for Calculating Permanent Magnetic Ring Bearings With Arbitrary Magnetization and Its Application to Optimal Bearing Design," in IEEE Transactions on Magnetics, vol. 50, no. 5, (2014), pp. 1-8

Mäkinen Antti J., Zetter Rasmus, Iivanainen Joonas, Zevenhoven Koos C. J., Parkkonen Lauri, and Ilmoniemi Risto J., "Magnetic-field modeling with surface currents. Part I. Physical and computational principles of bfieldtools", in *Journal of Applied Physics 128*, (2020)

Trumper D. L., Kim Won-Jong and Williams M. E., "Design and analysis framework for linear permanent-magnet machines," in *IEEE Transactions on Industry Applications*, vol. 32, no. 2, (1996), pp. 371-379

Zhang L. and Kou B., "Investigation of a novel 2-D Halbach magnet array for magnetically levitated planar motor," *2017 20th International Conference on Electrical Machines and Systems (ICEMS)*, (2017)